Application and limitations of inverted fireballs in a magnetron sputter device

J. Gruenwald [a],[*], M. Balzer [b], G. Eichenhofer [c], M. Fenker [b]

[a] Gruenwald Laboratories GmbH, Taxberg 50, 5660 Taxenbach, Austria
[b] fem Research Institute for Precious Metals and Metal Chemistry, Katharinenstraße 17, 73525 Schwäbisch Gmünd, Germany
[c] 4A-Plasma, Aichtalstr. 66, 71088 Holzgerlingen, Germany

ARTICLE INFO

ABSTRACT

In this paper the results of a first attempt to ignite an inverted fireball with a magnetron sputter source are presented. The conducted measurements show that there is no inverted fireball visible to the naked eye present during the experiments. However, some features are observed that indicate at least an initial onset of such an inverted fireball with an interruption before it is fully developed. In the course of the experiments magnetron sputtered molybdenum films have been deposited inside a highly transparent gridded anode and the obtained films have been analysed. It turns out that even without a visible inverted fireball being present, the film morphology and mechanical properties such as elastic modulus, hardness and surface roughness have changed significantly compared to a setup without inverted fireball anode. Additionally, the deposition rate is elevated by up to 20% inside the inverted fireball anode compared to the reference setup, although with a nearly threefold increase in total input power (cathode power + grid anode power). This increase in deposition rate was achieved despite the fact that a mesh electrode with only about 37% transparency was used. On the other hand, it was demonstrated that the use of additional gridded electrodes in such a device triggers instabilities and non-linearities in the plasma, which might be of interest for further fundamental research.

1. Introduction

Since their discovery about a decade ago, inverted fireballs (IFBs) have been studied for many reasons. While the first works about this plasma phenomenon were dedicated to instabilities [1–6] and basic plasma parameters [7–10], more recent work has focussed on studying their properties for surface treatment applications [11–14]. However, so far the experimental investigations regarding their usage in deposition processes were limited to PECVD techniques. An IFB comprises a dense plasma with very homogeneous plasma potential inside a highly transparent gridded anode. In order to ignite such an IFB, the positive potential on this anode has to be considerably higher than the ionisation potential of the working gas. If this condition is satisfied and the grid spacing of the mesh is about half a Debye length, closed equipotential surfaces are established around the anode [7]. This leads to the formation of a potential well, which efficiently traps ions and electrons inside the anode. Thus, the plasma density is raised by a factor of up to 15 in an IFB [11]. In combination with the homogeneous plasma potential that is created inside this Faraday cage, IFB plasmas contain an increased number of chemically active particles (i.e. ions and radicals). In this paper we report the first attempt to combine an IFB setup with a magnetron sputter cathode in a PVD machine with the aim of producing homogeneous molybdenum films inside the mesh anode. Furthermore, the results were compared to a 2D grid anode. It turned out that although no IFB was visible with the naked eye, some experimental observations can be related to the beginning ignition of an IFB. It was shown, for example, that introducing a closed, three dimensional anode with a high positive potential into the chamber leads to non-linearities and changes in the morphology and roughness of the obtained Mo films and, to a certain extent, the growth rates. However, it was also demonstrated that there are some problems related to this kind of anode configuration in magnetron sputtering devices. Firstly, the gridded IFB electrode, of course, becomes rapidly covered with sputtered material (at least on the side pointing towards the sputtering target). Secondly, the measurements suggest that an IFB setup, as it would be integrated in any PECVD system, shows a physical behaviour that is very similar to that of an anode assisted magnetron as it was reported by Münz and Zufrass [15] or to a ring anode in front of the magnetron as described by

Zdunek et al. and Chodun et al. [16,17] It has to be pointed out that at this point of our research, it remains unclear why some features of an IFB are observable, while others are absent despite the fact that currently known basic physical requirements for the formation of such a plasma are fulfilled. Thus, this paper should be seen as a starting point for further scientific discussion regarding the implementation of IFBs in PVD devices in general and in sputter chambers in particular. The paper itself will be organised as follows: The first section will be devoted to the description of the experimental setup. In the second section the main results will be presented and summarised and the last section will contain a discussion and some outlook on future experiments.

2. Experimental setup

Different sets of experiments were carried out in a stainless steel vacuum chamber for sputter deposition purposes. The measures of the Leybold L-560 UV chamber were 680/670/755 mm (width/depth/height) and it is equipped with a vacuum system consisting of a turbo-molecular and a rotary vane pump, which is capable of reaching a base pressure of 5×10^{-4} Pa. The measurements were conducted in an Ar atmosphere at 0.17 Pa and 0.52 Pa, respectively. A molybdenum target of 75 mm diameter with a purity of 99.95% was mounted with a central screw onto the balanced magnetron sputtering cathode. The power delivered to the sputtering cathode was 200 W using a medium frequency mode at 150 kHz (MKS ENI RPG-50). It was kept constant during all measurements except in oscillation measurements in Section 3.2, where the direct current (DC) mode and 300 W sputtering power were used. The electron temperatures (T_e) and plasma densities (n_e) for this magnetron sputtering cathode are usually in the order of 1 eV and 10^{10}/cm^3. These values correspond to a Debye length of 740 $\sqrt{(T_e/n_e)} = 74$ μm [18]. As an IFB electrode mesh should have a grid constant d of maximal twice the Debye length, a stainless steel grid with a grid constant of d = 50 μm (transparency of 37%) and a wire thickness of 30 μm was used in the experiments. This mesh was inserted into the sputter chamber in two configurations: Once as a closed rectangular prism (10 × 10 × 18 cm, Fig. 1 a) that was separated from the chamber floor with 0.8 mm thick dielectric space holders ("closed IFB anode"). The second configuration was just a 2D grid arranged in the same manner (10 × 18 cm, Fig. 1 b). Both versions were located 4 cm away from the magnetron. A negatively biased substrate holder (−50 V DC, Advanced Energy MDX-1) or a quartz crystal microbalance (QCM) with an eigenfrequency of 6 MHz were placed inside the prism or behind the 2D grid, respectively. Both were placed at a distance of 8 cm away from the sputtering cathode
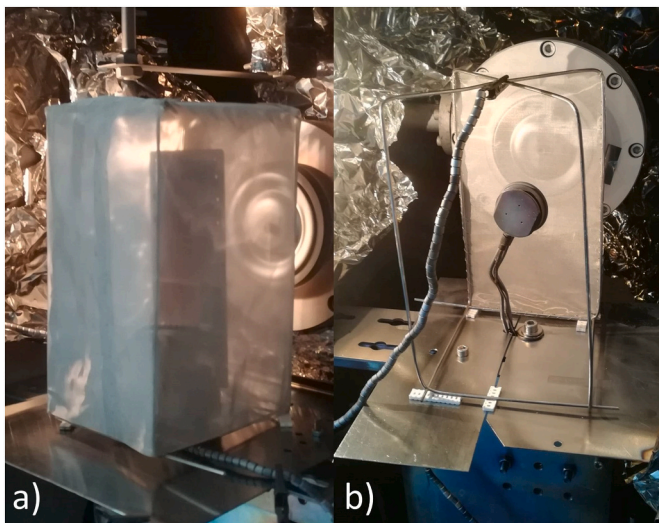

Fig. 1. Two different experimental setups: a) the closed IFB anode with substrate holder inside, and b) the 2D grid anode with QCM behind.

and aligned parallel to its surface. The anode was powered by an ADL GS-30-800 power supply, controlled by a MELEC SPIK 1000A HiPIMS pulser used in +DC mode, thus delivering positive DC voltages. All three power supplies (sputtering cathode, anode, substrate holder) were using the vacuum chamber as common ground. For the oscillation measurements, the voltage of the IFB was recorded by using an oscilloscope (Picoscope 2204). Both configurations are shown in Fig. 1 a) and b).

The film thickness was measured at artificial steps by tactile profilometry (MarSurf). The hardness of the 1 μm thick Mo coatings was measured by instrumented indention test (Fischer H100 xy p) with a maximum load of 4 mN with 10 s of load increase, hold at maximum load and decrease of load, respectively. Coating surfaces were characterized by Scanning Electron Microscopy (SEM) and Energy Dispersive X-ray spectroscopy (both Zeiss Auriga).

3. Results

This section will be divided into three subsections in order to give the different types of methods and measurements more structure. The subsections are devoted to electrical measurements, the observation of instabilities and the analysis of the obtained films.

3.1. Voltage, current and power measurements

The first measurements were conducted at two different pressure regimes in argon, namely at 0.17 Pa and at 0.52 Pa. The magnetron power was kept constant at 200 W while the bias voltage on the closed IFB anode was gradually increased. Although there was no IFB visible during the experiments, an increasing current that follows a power law was detected at higher anode voltages, both on the IFB grid and on the target electrode as to be seen in Fig. 2.

It has to be noted that both currents exhibit ranges of more or less linear growth and areas with an increase that follows a power law. Such an increase would be a sign of the ignition of an IFB, but since there is no visible light emanating from the anode, it might in this case also be attributed to additional ionisation processes outside the grid and sputtered material vapour. As the IFB anode introduces an additional electric field into the chamber, it alters the electric field that is produced by the target and changes its voltage as depicted in the following Fig. 3.

It can be seen from Fig. 3 that the target potential decreases with increasing IFB potential. There is a linear dependence of the anode voltage for values of more than 60 V vs. ground. The qualitative behaviour of the decreasing voltage is nearly identical for both pressure regimes. However, the value of the target potential remains higher at 0.17 Pa compared to the working pressure of 0.52 Pa. This is a strong indication that the plasma density between IFB anode and target is higher at higher pressure because higher electron densities improve the electrical shielding of the two electrodes. Elevated plasma densities also corroborate the assumption that the exponential part of the current increase at each electrode is most likely due to additional ionisation processes outside the mesh anode rather than due to additional ionisation processes achieved by an IFB. In the latter case the exponential increase would also mostly be observed in the current of the grid and not on the grid and target currents at the same time.

Additional measurements were carried out at a pressure 0.17 Pa with the closed IFB anode cage and with the 2D grid anode. The results are shown in the following Fig. 4 along with the standard deviation on the signal of the QCM.

It is evident from Fig. 4 a)–c) that the relation between IFB voltage and current and deposition rate (QCM signal) is practically identical with the behaviour of the 2D grid anode. This is interesting since the measurements show that the 2D grid draws somewhat more current at any given voltage than the closed cage, which has a much larger surface. Fig. 4 b) and c) show that below an anode voltage of about +200 V the deposition rate (QCM signal) of the IFB cage and the 2D grid are lower compared to conventional sputtering. This is attributed to the 37%
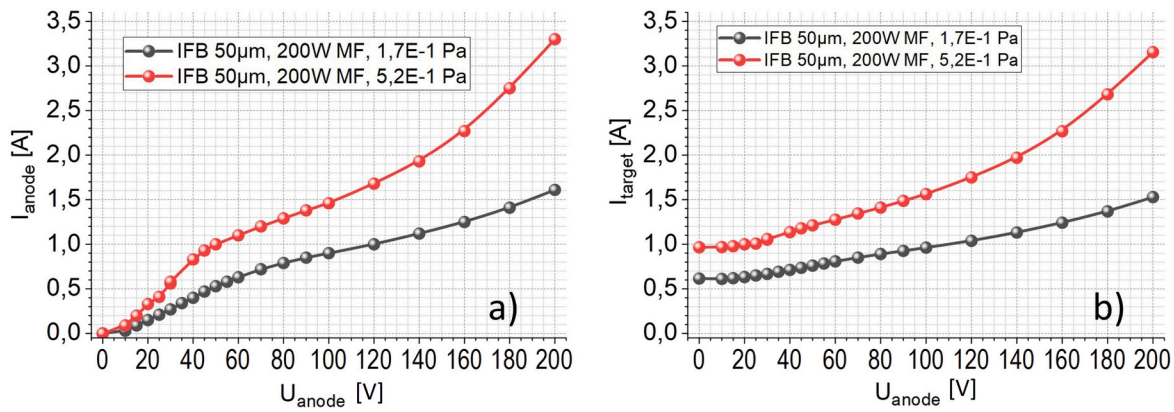
Fig. 2. IFB anode current [a)] and sputtering target current [b)] vs. IFB anode voltage, respectively.
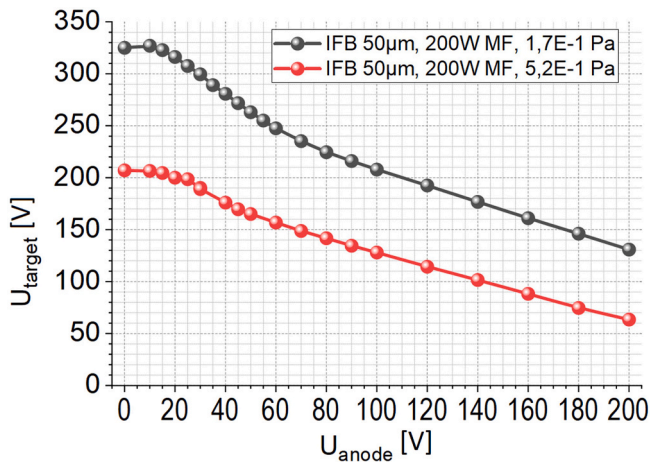

Fig. 3. Dependence of the target voltage on the anode voltage for pressures of 0.17 and 0.52 Pa, respectively.

transparency of the grid. Only at higher anode voltages a higher deposition rate is observed, which can be traced back to the higher total deposition power (target power + power at the anode), which leads to an increased target current as the target voltage nearly remains constant. At first glance it seems that the usage of a closed IFB grid electrode has no real impact on the experiments. However, Fig. 4 d) shows an interesting behaviour of the QCM signal: While its standard deviation drops significantly at biases of more than 275 V, the signal scattering increases exponentially for the closed IFB electrode. Oscillations measured on the grid voltage U(IFB) were studied and described in more detail in the following subsection.

3.2. Oscillations

Measurements with an oscilloscope attached to the IFB power supply revealed that the increase in dc voltage on the grid triggered a variety of oscillations. Some of those fluctuations are a significant sign of the occurrence of non-linearities inside the grid anode. The following Fig. 5 shows the different waveforms that were recorded on the IFB voltage at different anode bias voltages.

It is evident that the shape of the wave forms changes distinctly with increasing grid bias. Furthermore, there is a strong modulation of the oscillations. In order to gain a better insight into the changes a fast Fourier transformation (FFT) was done to distinguish the different frequencies. As it was known from previous experiments there are some frequencies that occur naturally in the system. These frequencies most probably stem from the measuring system and/or the plasma power

supplies of the magnetron and the anodes. In order to isolate these oscillations an FFT was also made without any voltage on the IFB grid (Fig. 5, "0 V"). This particular spectrum is presented in the following Fig. 6.

The measurements without any bias on the anode mesh ($U_{IFB} = 0$ V) reveal that there are three main frequencies present, namely the main frequency at 670 kHz and two more prominent oscillations at 740 kHz and 805 kHz, respectively. This and the following spectra were recorded at an Ar background pressure of 0.27 Pa while the sputter source was operated with 300 W in dc mode. As soon as the IFB voltage on the grid is turned on, this spectrum changes considerably with the largest changes at IFB voltages above +80 V vs. ground. Above this voltage an additional frequency band between 335 and 630 kHz appears, with a dominant peak at 510 kHz as shown in Fig. 7. The frequencies of these oscillations are too low to be connected to transit time or sheath-plasma instabilities of IFBs. Both of these types of waves would have frequencies that are several orders of magnitude higher than those observed in our experiments [1,2].

The appearance of additional frequencies is accompanied by the strong decrease of the 'natural' frequency amplitudes that are observed with increasing bias voltage on the anode. Especially the amplitude of the new main frequency at 510 kHz increases exponentially with increasing grid voltage, as depicted in Fig. 8.

This drastic increase in the amplitude of the 510 kHz oscillation in combination with the decrease of the naturally occurring frequencies indicates a transfer of energy into newly emerging oscillator modes. Another interesting fact is the emergence of a subharmonic oscillation at 335 kHz at increasing U_{anode} from 80 to 100 V while the power of the fundamental frequency at 670 kHz decreases. Such a shift to a sub-harmonic is usually connected to non-linearities in the oscillating system. In principle, such a behaviour has been observed in power electronic circuits or diode configurations [19].

Another interesting observation during our experiments was that there is no visible anode glow on the IFB grid as can be seen in the following Fig. 9.

It can be seen that the intensity of the magnetron glow in the background of Fig. 9 increases with increasing grid voltage but there is neither a visible anode glow nor an IFB present. This behaviour is continuing even at higher voltages up to about +200 V. Since the grid oscillations as well as the grid voltage and current could be measured without any problems, a faulty connection between the grid and the power supply can be ruled out.

3.3. Mo deposition on the IFB grid and substrate

The following Fig. 10 shows a magnified image of the IFB grid located in front of the target after about 3 h of deposition with 200 W magnetron power and various anode power between 0 and up to 700 W
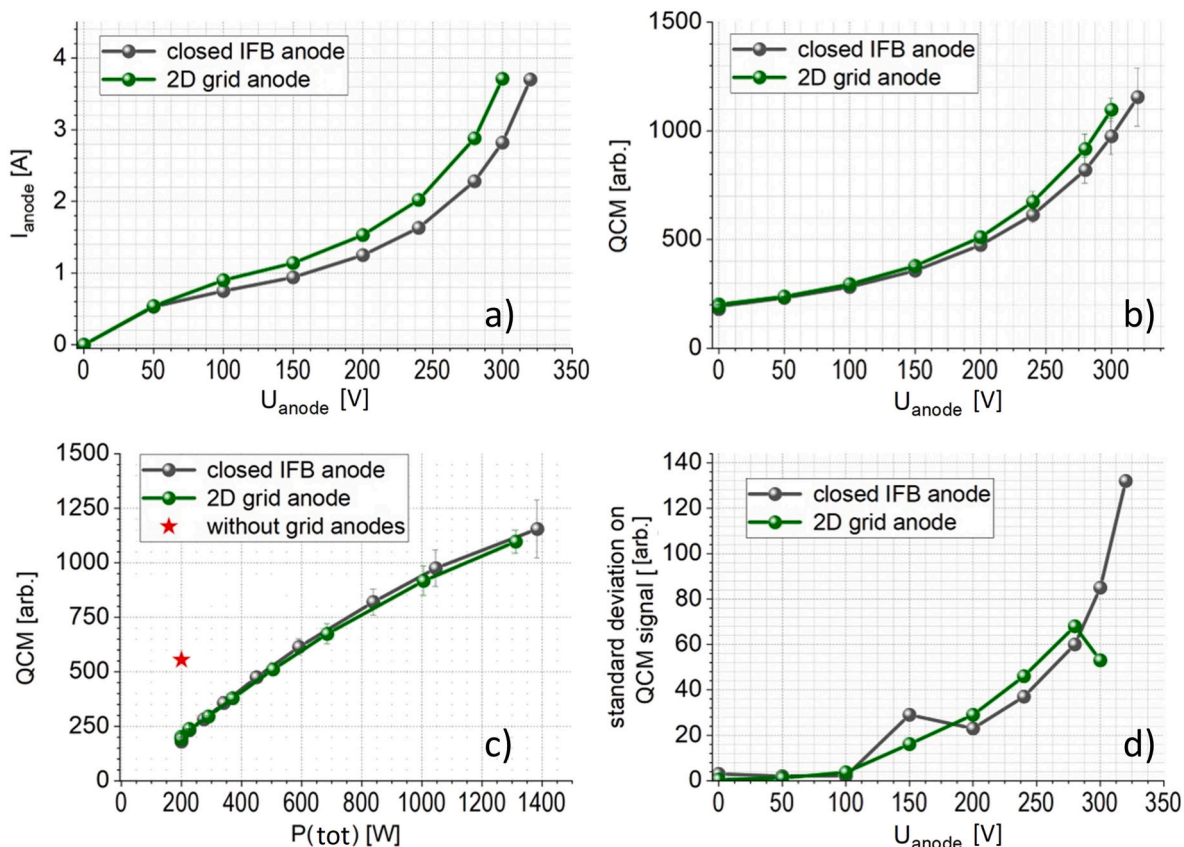
Fig. 4. Direct comparison of the performance of the closed IFB grid anode and the open 2D grid anode in terms of I-V characteristics [a)], the signal of the QCM as a function of anode voltage [b)], the total power P(tot) [c)], the red star represents a reference measurement without gridded anode, i.e. conventional set-up] as well as the standard deviation in the QCM signal [d)]. All measurements performed at a total pressure of 0.17 Pa and a target power of 200 W MF. The 2D grid anode was uncoated at the beginning of measurements shown, the closed IFB anode was slightly coated.
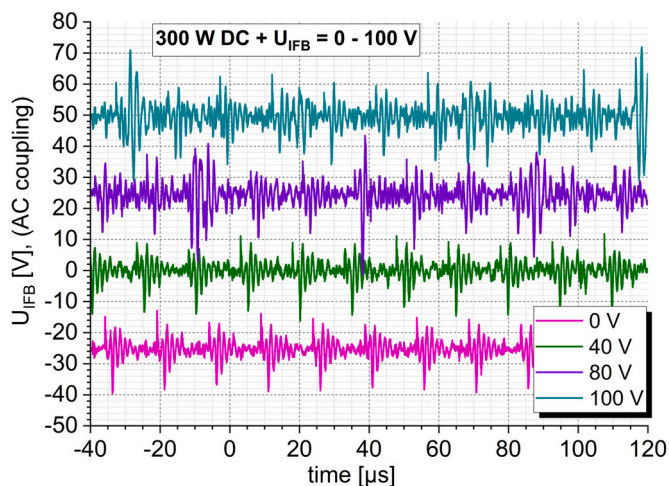

Fig. 5. Change in wave form shapes with increasing IFB grid voltage.

Fig. 6. Frequency spectrum of the oscillations picked up by the IFB grid without any voltage applied to it ($U_{IFB} = 0$ V).

(different experiments). During this time the 'window' area between the grid wires decreased from 2500 μm^2 to only 900 μm^2, which corresponds to a 64% reduction of transparency.

The right hand side of Fig. 10 shows a theoretical comparison between the decline in transparency of a mesh with 50 μm and one with 200 μm grid constant. It can be seen that the 200 μm mesh follows a nearly linear decrease in 'window' size during the first 40% of size reduction while the 50 μm mesh gets completely closed at the same time. The sides of the anode prism, on the other hand, are nearly unaffected by

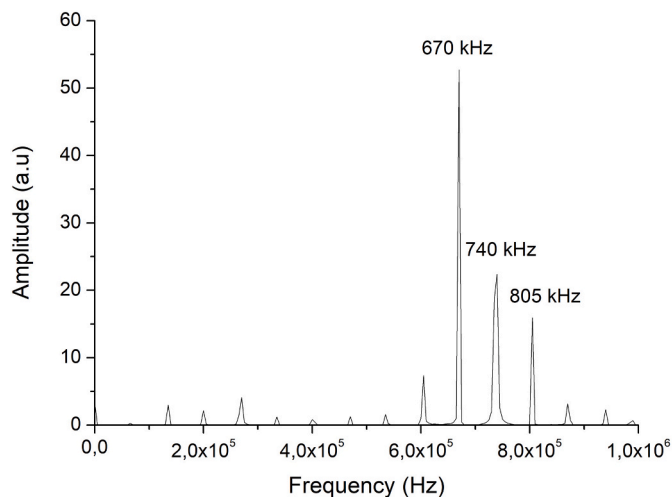coating with Mo, as the following Fig. 11 demonstrates.

This means that if an IFB could be successfully ignited in sputter devices, the sputter coating of the grid has to be taken into account. To a certain extend this should be possible, for example, by rotating the gridded anode during the deposition. Additionally, the grid constant should be taken as large as possible in order to keep the transparency high.
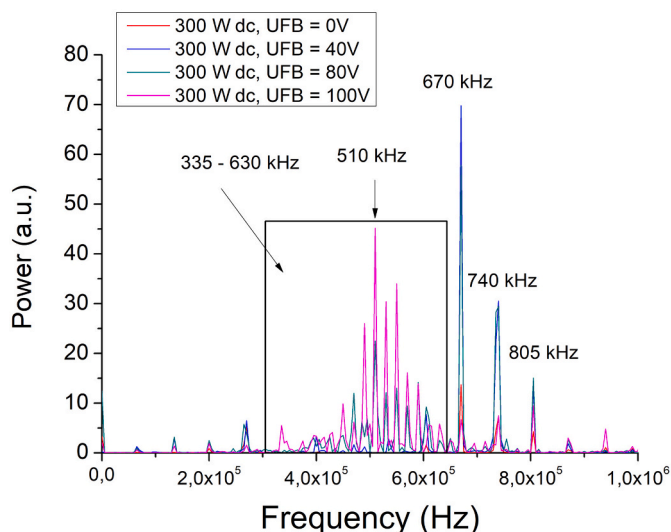
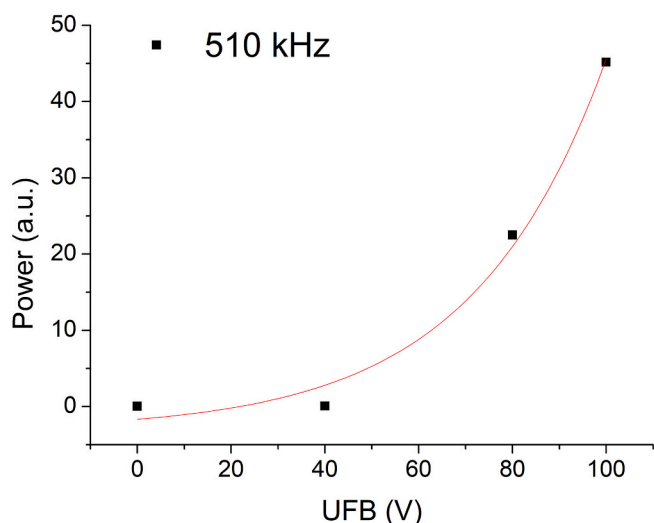**Fig. 7.** Spectra of oscillations on the IFB grid for different grid voltages.

Fig. 8. Amplitude of the 510 kHz frequency as a function of the grid voltage (red: exponential fit).

Finally, Mo films were deposited onto polished high speed steel at $p_{Ar} = 0.17$ Pa and investigated with respect to film morphology, hardness and Young's modulus and deposition rates. The results are presented in the following Figs. 12 and 13.

A comparison of the SEM surface images of the obtained Mo films could lead to the assumption that the surface roughness is decreased compared to a conventional magnetron sputter process when a closed IFB grid anode is used. However, the fracture cross sections show that

the roughness difference seems to be only marginal. In addition to the SEM images, EDX measurements were performed on the deposited films and no chemical elements other than molybdenum were found in the depositions. Hence, it can be concluded that the measured changes in the mechanical film properties are not due to incorporation of impurities.

For the Mo film deposited inside the closed IFB cage, the indentation hardness H_{IT} is increased by about 10%, while Young's modulus is decreased by about the same amount compared to the conventionally sputtered Mo film. Thus, the ratio H_{IT}^3/E_{IT}^2 is increased, suggesting a distinct increase in resistance to plastic deformation [20]. The deposition rate inside the IFB setup could be improved from 2.5 to 3.0 μm/h although with a nearly threefold increase in total input power. The change in film morphology is expected to be a result of a distinguishably increased current to the substrate (I_{bias}), which is increased from 6 to 10 mA when the IFB anode is applied. This substrate current must be caused by ionisation processes inside the closed IFB grid anode, as the anode potential prevents positive ions from the magnetron plasma to penetrate the grid. Therefore, the substrate current could be another sign for beginning ignitions of an IFB. Furthermore, it is interesting to point out that the sum of the potential on the anode and the magnetron is nearly constant in both cases (IFB and conventional setup). However, the total input power (Fig. 13, top row, second from left diagram) is nearly three times higher when a gridded anode is used at +240 V. This suggests that a considerable amount of additional current is drawn from the IFB anode, while the increase in substrate current within the IFB grid is only about two thirds. Since the total voltage, that is provided by the IFB anode and the magnetron is practically constant (Fig. 13, right upper bar chart) and so is the pressure and the working gas composition, it can be assumed that the grid anode enhances the number of ionisation processes between itself and the magnetron source, leading to higher electron densities and, thus, to higher grid currents. This anode-enhanced ionisation was already mentioned by Maidhof et al. [21], Münz and Zufrass [15] and in a patent from 2009 by Cremer and May [22]. The investigation of this assumption with optical emission spectroscopy is planned for the future and momentarily beyond the scope of this work.

4. Discussion and outlook

In this paper we report the first attempts to integrate an IFB setup into a PVD sputter chamber. So far a fully developed IFB could not be achieved. However, there are some indications that the onset of such a plasma phenomenon is imminent. The clearest signs of this are the onset of non-linearities, the increased substrate current and the change in film properties on the substrate inside the IFB anode. The most interesting features regarding the deposition with IFBs are an increased Vicker's hardness and a decreased surface roughness. Those features are a consequence of the IFB setup, which increased the current to the substrate. This is also corroborated by the fact that ions, which are created outside the IFB anode, cannot penetrate the grid potential. Hence, there must be additional ionisation processes inside the grid prism that enhance the substrate current. As increased hardness and surface
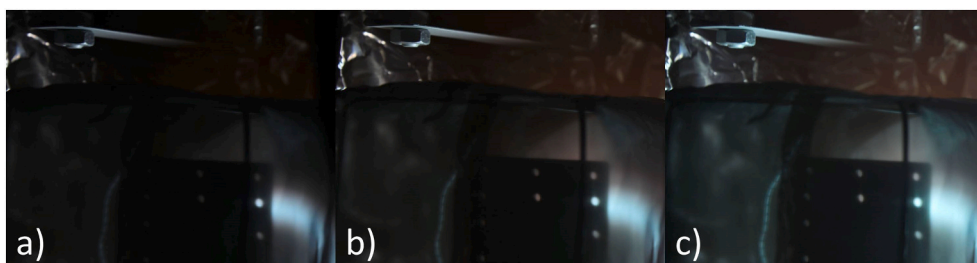

Fig. 9. Photographs of the IFB anode (magnetron in the background) at 0.52 Pa in Ar at U(anode) = 0 (a), +40 V (b) and +100 V (c).
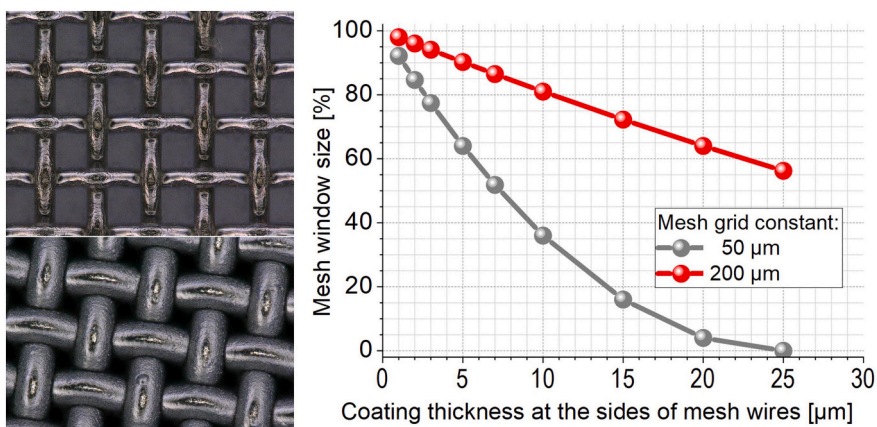
Fig. 10. Magnified view on the IFB mesh before the measurements (left, top) and after 3 h of deposition experiments (left, bottom). Right: calculated decrease in mesh window size as a function of the wire thickness for the experimental parameters described in this paper.
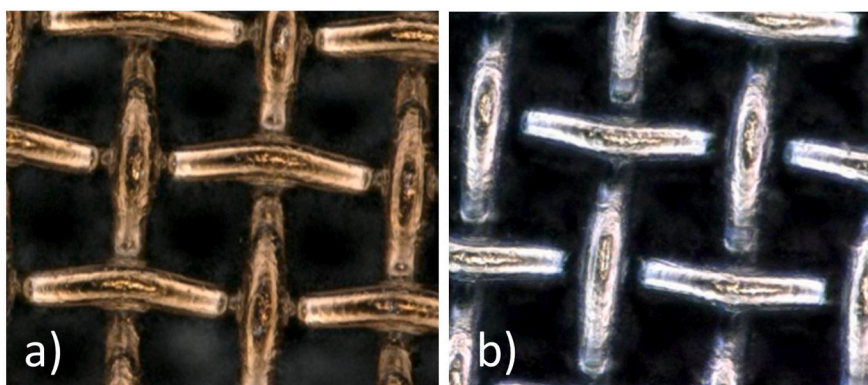

Fig. 11. Images from the other sides of the IFB grid. The back side opposite the magnetron [a)] and one of the grid sides perpendicular to the front/back [b)].
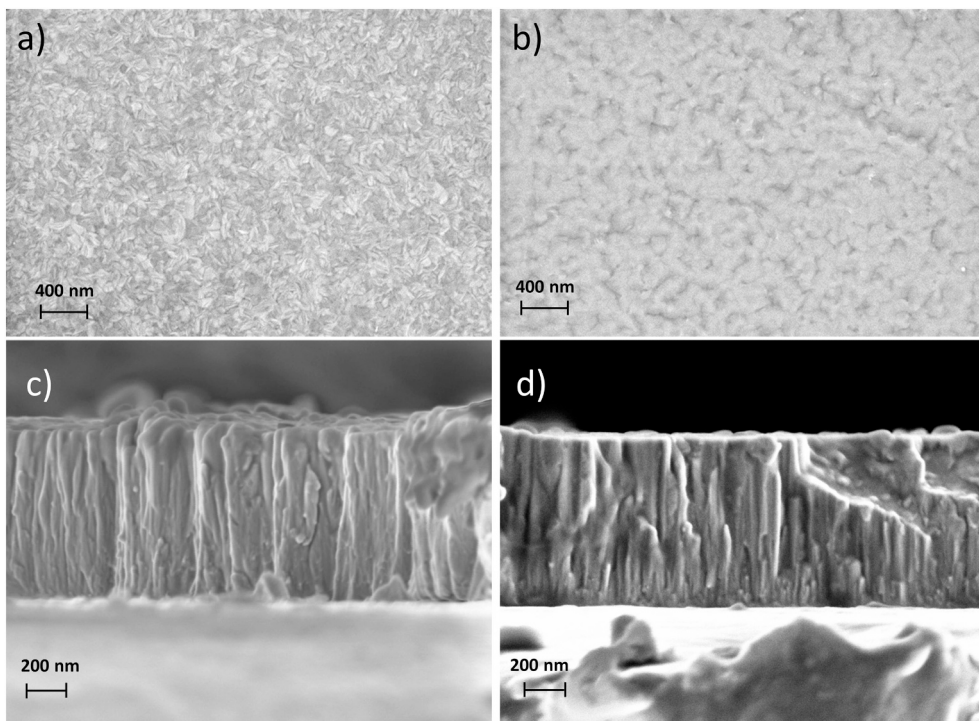

Fig. 12. SEM images of a conventionally sputter-deposited Mo film [a) and c)] and the film obtained inside the IFB anode [b) and d)]. Note that c) and d) have about twice the magnification of a) and b). Upper row show SEM surface images, bottom row SEM fracture cross sections of the Mo films.
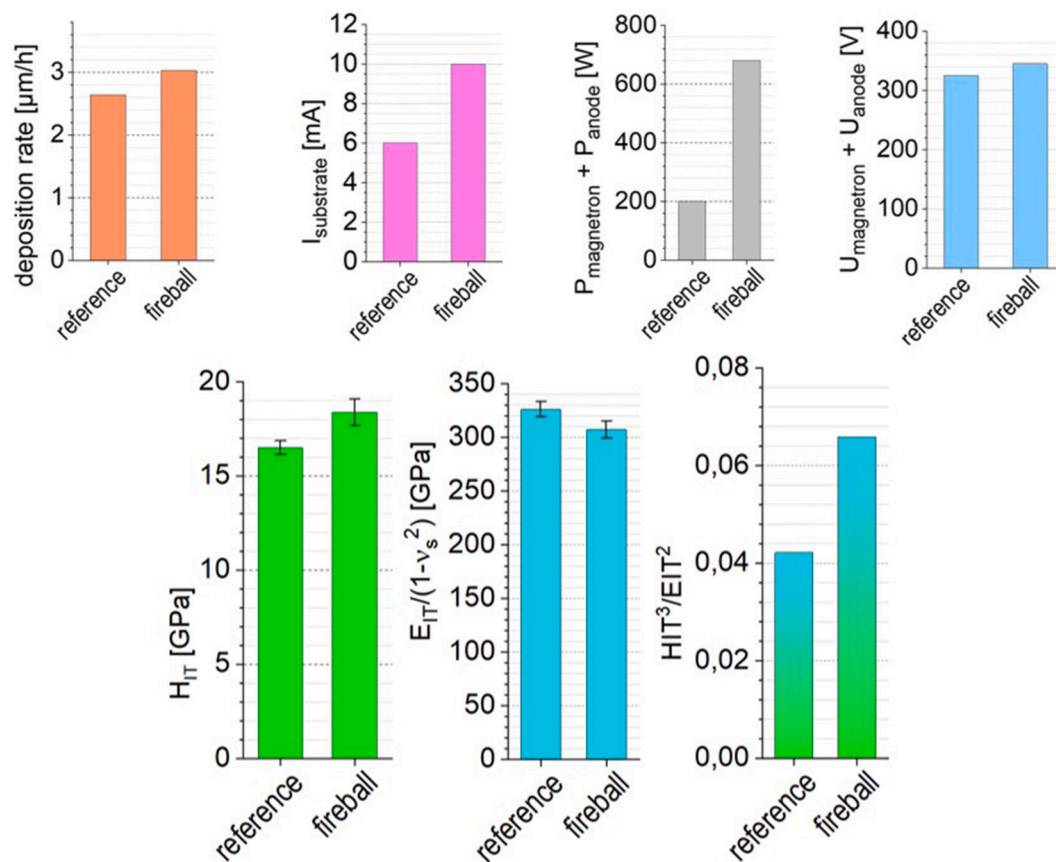
Fig. 13. Summary of the most important deposition parameters and mechanical properties of the sputter coated films. Top row, from left to right: deposition rate, current to substrate, total input power and sum of input voltages. Bottom row, from left to right: indention hardness H_{IT} (0,004 10/10/10), Young's modulus E_{IT} and H_{IT}^3/E_{IT}^2 ratio.

smoothness are favourable for a variety of technical applications, the IFB configuration should be studied further. However, there are several problems that have to be addressed in order to combine IFB electrodes with conventional magnetron sputter sources: the rapid coating of the grid anode has to be prevented and the transparency of the mesh has to be increased as much as possible, also to increase the particle currents to the substrate and make the process more energy efficient. It can be concluded that the use of closed gridded anodes changes the film properties to some extend even when an IFB cannot be seen with the naked eye. The reason why an IFB was not fully developed, could not be determined within the measurements presented in this paper and speculations in these directions are beyond the scope of this work. Thus, further investigations are planned for the future (e.g. it will be studied if there is in fact an IFB present that only emits light in the UV and/or IR range). This will be done, amongst other techniques, with optical emission spectroscopy, which will also allow more insight into the excitation and ionisation states of the Ar and Mo atoms that are present during the sputter deposition process. It is also planned to investigate possible remedies against the rapid coating of the IFB anode and further increases in the deposition rate.

CRediT authorship contribution statement

J. Gruenwald: Writing – original draft, Investigation, Formal analysis, Conceptualization. **M. Balzer:** Conceptualization, Investigation, Resources, Formal analysis. **G. Eichenhofer:** Project administration, Conceptualization. **M. Fenker:** Supervision, Conceptualization, Project administration, Investigation, Formal analysis.

Declaration of competing interest

The authors declare that they have no known competing financial interests or personal relationships that could have appeared to influence the work reported in this paper.

References

[1] R.L. Stenzel, et al., Transit time instabilities in an inverted fireball. I. Basic properties, Phys. Plasmas 18 (1) (2011), 012104.
[2] R.L. Stenzel, et al., Transit time instabilities in an inverted fireball. II. Mode jumping and nonlinearities, Phys. Plasmas 18 (1) (2011), 012105.
[3] R. Bandara, J. Khachan, Nonlinear saturation of the ion-electron Buneman instability in a spherical positively pulsed gridded inertial electrostatic confinement device, Phys. Plasmas 22 (8) (2015), 082701.
[4] V. Mitra, et al., Mixed mode oscillations in presence of inverted fireball in an excitable DC glow discharge magnetized plasma, Phys. Plasmas 24 (2) (2017), 022307.
[5] J. Gruenwald, On the dispersion relation of the transit time instability in inverted fireballs, Phys. Plasmas 21 (8) (2014), 082109.
[6] J. Gruenwald, C. Teodorescu, On the dispersion relation for the Buneman instability in spherically confined plasmas, Plasma Phys. Controlled Fusion 61 (3) (2019), 035007.
[7] J. Gruenwald, et al., Further experiments on inverted fireballs, in: Proc. 38th EPS Conf. Plasma Phys, 2011.
[8] J. Gruenwald, J. Reynvaan, P. Geistlinger, Basic plasma parameters and physical properties of inverted He fireballs, Plasma Sources Sci. Technol. 27 (1) (2018), 015008.

[9] J. Gruenwald, J. Reynvaan, P. Geistlinger, Influence of inhomogeneous electrode biasing on the plasma parameters of inverted H2 fireballs, J. Technol. Space Plasmas 1 (1) (2020) 1–4.

[10] D. Levko, J. Gruenwald, On the energy deposition into the plasma for an inverted fireball geometry, Phys. Plasmas 24 (10) (2017), 103519.

[11] P. Knoll, et al., PECVD of carbon by inverted fireballs: from sputtering, bias enhanced nucleation to deposition, Diam. Relat. Mater. 65 (2016) 96–104.

[12] M. Mayer, et al., Diamond like carbon deposition by inverted fireballs, Mater. Today Proc. 3 (2016) S184–S189.

[13] J. Reynvaan, et al., Multiple fireballs in a reactive H_2/CH_4 plasma, IEEE Trans. Plasma Sci. 42 (10) (2014) 2848–2849.

[14] J. Gruenwald, J. Reynvaan, P. Knoll, Creation and characterization of inverted fireballs in H_2 plasma, Phys. Scr. 2014.T161 (2014), 014006.

[15] W.D. Münz, T. Zufrass, Industrial scale deposition of well adherent superhard and low friction C-DLC coatings grown by HIPIMS and anode assisted unbalanced magnetron sputtering, Surf. Coat. Technol. 387 (2020) 125485.

[16] K. Zdunek, et al., Characterization of sp3 bond content of carbon films deposited by high power gas injection magnetron sputtering method by UV and VIS Raman spectroscopy, Spectrochim. Acta A Mol. Biomol. Spectrosc. 194 (2018) 136–140.

[17] R. Chodun, et al., Multi-sided metallization of textile fibres by using magnetron system with grounded cathode, Mater. Sci.-Pol. 35 (3) (2017) 639–646.

[18] F.F. Chen, Introduction to Plasma Physics, Springer Science & Business Media, 2012.

[19] J.H.B. Deane, D.C. Hamill, Instability, subharmonics and chaos in power electronic systems, in: 20th Annual IEEE Power Electronics Specialists Conference, IEEE, 1989.

[20] J. Musil, M. Jirout, Toughness of hard nanostructured ceramic thin films, Surf. Coat. Technol. 201.9-11 (2007) 5148–5152.

[21] H. Maidhof, et al., Developments in decorative coatings, in: Society of Vacuum Coaters 39 th Annual Technical Conference, 1996.

[22] R. Cremer, W. May, Apparatus and Method for Pretreating and Coating Bodies, U.S. Patent No. 9,812,299., 7 Nov. 2017.